IMMUNOTHERAPY OF EXPERIMENTAL MELANOMA WITH ICOS-Fc LOADED IN BIOCOMPATIBLE AND BIODEGRADABLE NANOPARTICLES.

Clemente Nausicaa[a,1], Boggio Elena[a,1], Gigliotti Casimiro Luca[a,1], Raineri Davide[a,b], Ferrara Benedetta[c], Miglio Gianluca[c], Argenziano Monica[c], Chiocchetti Annalisa[a,b], Cappellano Giuseppe[a,b], Trotta Francesco[d], Caldera Fabrizio[d], Capucchio Maria Teresa[e], Yagi Junji[f], Rojo Josè Maria[g], Renò Filippo[a], Cavalli Roberta[c,*], Dianzani Chiara[c], Dianzani Umberto[a,b]

[a]Department of Health Sciences, Inter Interdisciplinary Research Center of Autoimmune Diseases, UPO, 28100 Novara, Italy

[b]Center for Translational Research on Autoimmune and Allergic Disease—CAAD, Università del Piemonte Orientale, 28100 Novara, Italy

[c]Department of Scienza e Tecnologia del Farmaco, University of Torino, 10125 Torino, Italy

[d]Department of Chemistry, University of Torino, 10125 Torino, Italy

[e]Department of Veterinary Sciences, University of Torino, 10095 Grugliasco (TO), Italy

[f]Department of Microbiology and Immunology, Tokyo Women's Medical University, Tokyo 108-8639, Japan

[g]Departamento de Medicina Celular y Molecular, Centro de Investigaciones Biologicas, Consejo Superior de Investigaciones Cientıficas, 28040 Madrid, Spain

[1]Clemente Nausicaa, Boggio Elena and Gigliotti Casimiro Luca equally contributed to this work.

*Corresponding author. E-mail address: roberta.cavalli@unito.it; Department of Scienza e Tecnologia del Farmaco, University of Torino, 10125 Torino, Italy

GRAPHICAL ABSTRACT

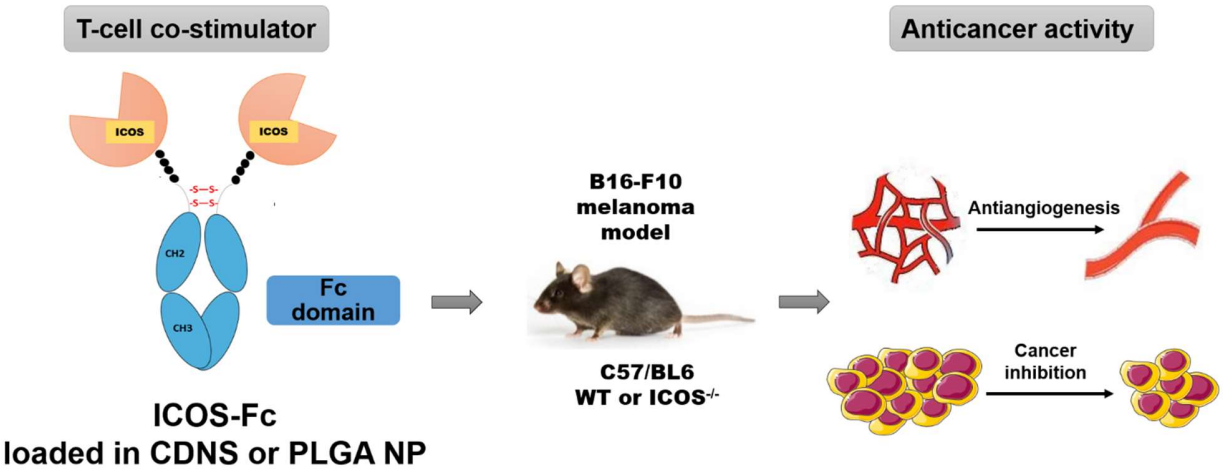

ABSTRACT

Inducible T-cell costimulator (ICOS) upon binding to its ligand (ICOSL) mediates adaptive immunity and antitumor response. Thus, antitumor therapies targeting the ICOS/ICOSL pathway hold great promise for cancer treatment. In this regard, ICOSL triggering by a soluble recombinant form of ICOS (ICOS-Fc) hampered adhesiveness and migration of dendritic, endothelial, and tumor cells *in vitro*. Furthermore, *in vivo* treatment with ICOS-Fc previously showed the capability to inhibit lung metastatization of $ICOSL^+$ B16-F10 melanoma cells when injected intravenously in mice, but it failed to block the growth of established subcutaneous B16-F10 murine tumors. Thus, we asked whether passive targeting of solid tumors with ICOS-Fc-loaded biocompatible and biodegradable nanoparticles (NPs) could instead prove effectiveness in reducing tumor growth. Here, ICOS-Fc was loaded in two types of polymer nanoparticles, i.e. cross-linked β-cyclodextrin nanosponges (CDNS) and poly(lactic-co-glycolic acid) (PLGA) NPs and *in vitro* characterized. *In vivo* experiments showed that treatment of C57BL6/J mice with ICOS-Fc loaded into the two nanoformulations inhibits the growth of established subcutaneous B16-F10 tumors. This anticancer activity appears to involve both anti-angiogenic and immunoregulatory effects, as shown by decreased tumor vascularization and downmodulation of IL-10 and Foxp3, two markers of regulatory T cells (Tregs). Overall, the substantial *in vivo* anticancer activity of ICOS-Fc-loaded CDNS and PLGA NPs against different components of the tumor microenvironment makes these nanoformulations attractive candidates for future combination cancer therapy.

Keywords

β-cyclodextrin nanosponges, PLGA nanoparticles, ICOS-L, melanoma, controlled release

1. Introduction

ICOS is a T-cell costimulatory molecule first described by our group as H4 [1,2] and then cloned by Hutloff and co-workers as a molecule belonging to the CD28 family, which we subsequently proved to be identical to H4 [3,4]. A distinctive feature of ICOS is its selective expression in activated T cells, but it has also been recently detected in dendritic cells (DCs) [5]. ICOS binds to ICOS-ligand (ICOSL, also named B7RP-1, B7-H2, B7-like protein Gl50, GL50, KIAA0653, LICOS, or CD275), expressed by several cell types, such as DCs, macrophages, B cells, endothelial cells (ECs), epithelial cells, and fibroblasts [6].

ICOS triggering regulates T-cell activation in lymphoid organs and T-cell function at inflammation sites by supporting the differentiation of regulatory T cells (Tregs) and type 17 T helper (Th17) cells. Moreover, it modulates follicular T helper cell function and $CD8^+$ cell-mediated response to tumors and intracytoplasmic pathogens [7-11]. It also regulates the development of germinal centers in secondary lymphoid tissues, and its deficiency causes common variable immunodeficiency [9].

A striking increase in the number of $ICOS^+$ effector T cells has been reported in melanoma patients treated with anti-CTLA-4 antibodies (Abs) to achieve antitumor immune response, suggesting that the ICOS/ICOSL pathway is essential for anti-CTLA-4 Ab-mediated anticancer activity. In good agreement, the therapeutic efficacy of anti-CTLA-4 Abs was strongly reduced in $ICOS^{-/-}$ mice [12]. More recently, the ICOS/ICOSL pathway has also been shown to play a role in colorectal cancer pathogenesis since ICOSL is expressed on tumor cells, and ICOS expression levels on tumor-infiltrating T cells correlated with patient survival [13].

The ICOS-ICOSL interaction triggers bidirectional signals modulating the response of ICOSL-expressing cells. In mouse DCs, for instance, ICOS-mediated “reverse signaling” increases interleukin (IL)-6 secretion [14]. Moreover, we have shown that ICOSL triggering by a bivalent soluble form of ICOS, consisting of the Fc portion of IgG1 and two molecules of the extracellular portions of ICOS

(ICOS-Fc), modulates the function of several human cell types. In ECs and DCs, it inhibits adhesiveness and migration [15-17]. In DCs, it can also modulate cytokine secretion by increasing production of IL-23 while promoting antigen cross-presentation *in vitro* [15]. Moreover, it inhibits osteoclast differentiation from monocytes and the bone resorption activity of mature osteoclasts [18].

At the molecular level, ICOSL downstream signaling leads to dephosphorylation of ERK and p38 in ECs and downregulation of β-Pix expression in DCs and tumor cells [15-17]. Others have reported cross-talk between ICOSL and several pattern recognition receptors in human DCs through a signaling pathway involving RACK1, PKC and JNK [5]. In human tumor cell lines expressing ICOSL, treatment with ICOS-Fc inhibits cell adhesiveness, migration, and epithelial-mesenchymal transition and induces dephosphorylation of FAK and down-modulation of β-Pix [16]. In this regard, we have observed a similar inhibition of migration in several tumor melanoma cell lines and in a primary melanoma cell line (16 and unpublished data). Altogether, these data suggest that ICOSL triggering by ICOS-Fc may exert anti-tumor effects by acting on both tumor cells and cells localized in the tumor microenvironment, such as DCs, ECs, and macrophages.

The aforementioned *in vitro* findings have been supported by *in vivo* studies showing that ICOS-Fc treatment remarkably inhibits the development of experimental lung metastases upon injection of B16-F10 melanoma cells in the tail vein of syngenic mice. Moreover, using a xenograft model of human CF-PAC1 cell line injected in the tail vein of NOD-SCID-IL2Rγnull (NSG) mice, we have previously shown that optimal inhibition of metastasization requires concomitant treatment with human and mouse ICOS-Fc. Thus, these findings support a model whereby ICOS-Fc exerts its inhibitory effect on metastatic dissemination by acting on both human tumor cells and the mouse environment [16].

By contrast, we have been unable until now to detect any effect of ICOS-Fc treatment on the growth of established tumors despite extensively testing several doses and delivery routes of ICOS-Fc (e.g. intravenous, intraperitoneal, or peritumoral injection) and a number of experimental models of

tumor expressing ICOSL (unpublished results). These negative results might be partly explained by an inefficient *in vivo* biodistribution of ICOS-Fc that, despite being sufficient to induce deleterious effects on the systemic anti-tumor immune response, would reduce its therapeutic effect in the tumor microenvironment.

Nanotechnology-based drug delivery systems have been emerged as effective tools to optimize both biodistribution and cytotoxicity of chemotherapeutic agents. Indeed, loading antineoplastic drugs into different types of nanoparticles (NPs) allows to deliver higher drug amount directly into the tumor than the solution with relatively low systemic concentration, thereby strengthening drug cytotoxicity and minimizing its adverse effects. This NP feature is related to the ability to passively accumulate into the tumors through the so-called enhanced permeability and retention (EPR) effect [19,20]. Moreover, nanoparticles can enhance the intracellular uptake of drugs.

NPs are known to protect drugs from enzymatic and chemical degradation during systemic circulation while substantially reducing non-specific delivery. This aspect is particularly important for biomacromolecules, being susceptible to chemical and physical degradation and instability at all stages of manufacturing, storage, and administration. Moreover, biomacromolecules exhibit a complex molecular structure with a high molecular weight and amphiphilic/hydrophilic nature, both of which hinder their penetration into cells. Thus, nanoparticle formulations represent a new avenue for optimizing both delivery and tumor cell kill of anticancer macromolecules such as ICOS-Fc [21,22].

The aim of this work was to optimize ICOS-Fc effectiveness and tumor targeting and delivery through NP technology. The goal was to show that *in vivo* injection of ICOS-Fc-loaded NPs can inhibit tumor growth of established B16-F10 tumors. In particular, we *in vitro/in vivo* characterized β-cyclodextrin nanosponges (CDNS), which are polymer nanoparticles obtained by cross-linking cyclodextrins with suitable cross-linker. Interestingly, CDNS demonstrated the capability to store and

protect biomacromolecules. For comparison, poly(lactic-co-glycolic) acid (PLGA) NPs have been also studied as ICOS-Fc nanocarriers.

2. Materials and Methods

2.1. Cells

B16-F10 melanoma cells (ATTC, Manassas, VA, USA) were grown in RPMI plus 10% FCS, 100 U/ml penicillin, and 100 μg/ml streptomycin (complete medium) at 37°C in a 5% CO_2 humidified atmosphere. Human umbilical vein endothelial cells (HUVECs) were isolated from human umbilical veins *via* trypsin treatment and cultured as previously reported [23]. The use of HUVECs was approved by the institutional review board of the "Presidio Ospedaliero Martini" of Turin (Prot. 263-07/NF) and conducted in accordance to the Declaration of Helsinki.

2.2. β-cyclodextrin nanosponges synthesis

β-cyclodextrin nanosponges (CDNS) were prepared by crosslinking β-cyclodextrin (kindly provided by Roquette Frères) with pyromellitic dianhydride (Sigma-Aldrich, Saint Louis, MO, USA), in a 1:4 molar ratio. Synthesis was carried out in a 100 ml round bottom flask at room temperature for 24 h. Specifically, 6.108 g of β-cyclodextrin were stirred in 25 ml of anhydrous dimethyl sulfoxide (Sigma-Aldrich) till it was completely dissolved. Afterwards, 6.3 ml of triethylamine (Sigma-Aldrich) and 4.695 g of pyromellitic dianhydride were added under intense stirring. In a few minutes, a rigid gel was formed. In the following days, CDNS was ground in a mortar and washed with an excess of deionized water through Buchner filtration. Finally, CDNS purification by means of Soxhlet extraction in acetone for 24 h was performed and then CDNS were dried at room temperature.

2.3. Preparation of CDNS nanoformulations

To obtain a nanoformulation suitable for *in vivo* administration, a nanosponge nanosuspension was prepared using a purposely tuned top down method. For this purpose, CDNS were suspended in saline solution (NaCl 0.9%) at the concentration of 10 mg/ml and firstly homogenized using a high shear homogenizer (Ultraturrax) for 10 min at 24000 rpm. Then, CDNS suspension underwent size reduction by high pressure homogenization (HPH), using a high pressure homogenizer (EmulsiFlex C5, Avastin) for 90 min at a back-pressure of 500 bar. The nanosuspension obtained was then purified by dialysis (membrane cutoff 12000 Da) to eliminate potential synthesis residues.

2.4. Preparation of ICOS Fc-loaded CDNS

To obtain ICOS-Fc-loaded CDNS, ICOS-Fc was added under stirring to the aqueous nanosuspension of pre-formed CDNS at the concentration of 1 mg/ml. Then, the mixture was gently stirred at room temperature for 2 h. Finally, a purification step by dialysis (membrane cutoff 50 KDa) was carried out to eliminate unbounded ICOS-Fc.

2.5. Poly(lactic-co-glycolic acid) nanoparticle preparation

Poly(lactic-co-glycolic acid) nanoparticles (PLGA NPs) were prepared by a modified double solvent evaporation method [24]. Briefly, 60 mg of PLGA 65:35 crystals (Sigma-Aldrich) were dissolved in 1ml of dichloromethane (DCM, Sigma-Aldrich) at room temperature, and after adding 50 µl of PBS the solution was sonicated at a constant pulse for 1 min (power 0.21). Five volumes of 1% polyvinyl alcohol (PVA, Sigma-Aldrich) aqueous solution were carefully added to the resulting emulsion in order to maintain phase separation. A further 2 min, sonication was performed to obtain the final emulsion, which was then evaporated overnight under a fume hood to remove DCM. The resulting NPs were washed 7x in distilled water by centrifugation at 8,000 rpm for 10 min and resuspended in NaCl 0.9%, and stored at 4°C. NP-containing ICOS-Fc were produced as above by adding ICOS-Fc ─ 1 mg was

lyophilized and then resuspended in 50 µl of PBS ─ to the PLGA solution dissolved in DCM just before sonication.

2.6. Characterization of CDNS and PLGA NP formulations

After dilution in water, the average diameter and polydispersity index (PDI) of blank and ICOS-Fc-loaded CDNS and PLGA NPs were determined by photon correlation spectroscopy (PCS) using a 90 Plus Instrument (Brookhaven, NY, USA) at a fixed angle of 90° and a temperature of 25 °C. Each sample was analyzed in triplicate. The sample zeta potentials were measured by electrophoretic mobility (90 Plus Instrument, Brookhaven, NY, USA). For zeta potential determination, samples were diluted in water and placed in the electrophoretic cell, where an electric field of approximately 15 V/cm was applied. The morphology and particle size in the dry state of CDNS and PLGA NPs were studied using a field-emission scanning electron microscopy (FESEM, JEOL-JSM-6700F). After metallization with chromium, the samples were observed up to 100.00 KX, by applying an EHT voltage of 3.00 kV and a probe current of 100 pA. Blank and ICOS-Fc-loaded CDNS and PLGA NP size distribution was determined by Nanosight – Nanoparticle Tracking Analysis (NTA). An NS300 NanoSight (Malvern Instrument, Worcestershire, UK) fitted with a NS300 flow-cell top plate and a 532 nm laser was used. Data were analyzed on the NTA software 3.2 (Malvern Instrument, Worcestershire, UK). CDNS and PLGA NP formulations were diluted in saline solution (0.9% NaCl) 1:100000 immediately before analysis and loaded into the sample chamber prior to video recordings. Each analysis was replicated three times for each sample.

2.7. ICOS-Fc quantitative determination

ICOS-Fc concentration was determined using the Pierce™ BCA Protein Assay Kit (Thermo Scientific, Rockford, IL USA). This colorimetric assay is based on the reduction of Cu^{+2} to Cu^{+1} by

protein in an alkaline medium, which is detected using the bicinchoninic acid (BCA) reagent. The chelation of two molecules of BCA with one cuprous ion (Cu^{+1}) formed a purple-colored reaction product, which exhibited a strong absorbance at 562 nm. One ml of the mixture of reagents A (BCA) and B (alkaline solution), in a ratio of 1:50, was added to the samples. The samples were then incubated for 30 min at 37 ° C for the reaction to take place.

2.8. Loading capacity and encapsulation efficiency of CDNS and PLGA NPs

Weighted amounts of freeze-dried ICOS-Fc-loaded CDNS and PLGA NPs were dispersed in 5 mL of water. After sonication and centrifugation, the supernatants were analyzed by BCA Protein Assay and the concentration of ICOS-Fc in CDNS and PLGA NPs quantified. The loading capacity of the ICOS-Fc loaded CDNS and PLGA NPs was calculated using the following equation: Loading capacity = [amount of ICOS-Fc/ weight of NP] x 100. The encapsulation efficiency was calculated according to the equation: Encapsulation efficiency = [amount of ICOS-Fc encapsulated/ total amount of ICOS-Fc] x 100.

2.9. In vitro release kinetics of ICOS-Fc from CDNS and PLGA NPs

The *in vitro* release study was carried out according to the dialysis bag technique. The donor phase, consisting of 2 ml of ICOS-Fc-loaded CDNS or ICOS-Fc-loaded PLGA NP nanosuspension (1 mg/ml), was placed in a dialysis bag (cellulose dialysis membrane, cut off 100KDa, Spectrapore) and was dialyzed against 20 ml of receiving medium, consisting of phosphate-buffered saline (PBS) at pH 5.5 or 7.4. At fixed times, 1 ml of the receiving phase was withdrawn and replaced with fresh medium. The samples collected were analyzed by BCA assay. The experiments lasted five days (n=3).

The *in vitro* release kinetics of ICOS-Fc from CDNS was fitted to four mathematical kinetic models (i.e. zero-order kinetic model, first-order kinetic model, simplified Higuchi model and Korsmeyer–Peppas

model) to determine the highest correlation with the experimental release results. For each model, the rate constant and correlation values were calculated by applying a linear regression fit.

2.10. In vitro evaluation of ICOS-Fc stability over time

The *in vitro* stability of ICOS-Fc loaded in CDNS and PLGA NPs suspended in a PBS solution at pH 7.4 was evaluated by measuring ICOS concentration over time using the BCA assay, as described above. An ICOS-Fc PBS solution at pH 7.4 was used as a control. The samples were stored at 4°C and analyzed after 0, 1, 7, 14, 28, 60, and 90 days. To determine ICOS-Fc concentration, 100 µl of ICOS-Fc loaded CDNS or PLGA NP samples were withdrawn at each time and diluted in filtered water. After sonication for 15 min and centrifugation (10000 rpm, 10 min), the supernatant was analyzed by BCA assay.

Moreover, the *in vitro* stability of ICOS-Fc loaded nanoformulations was investigated by determining their sizes and ICOS concentration after 48 h of incubation either at 25 °C or at physiological temperature (37 °C).

2.11. Cell viability assay

B16-F10 cells were seeded in 96-well plates at $1x10^3$ cells/well in complete RPMI-1640 medium. After 24 h, the medium was removed, and the cells were incubated for 48 h in the medium containing titrated amounts (0.5-5 µg/ml) of CDNS or PLGA NPs. After 72 h of incubation, viable cells were evaluated by adding 2,3-bis[2-methoxy-4-nitro-5sulfophenyl]-2H-tetrazolium-5carboxanilide (MTT, Sigma-Aldrich) inner salt reagent (0.5 mg/ml) for 4 h at 37°C. Then, the MTT solution was discarded and formazan crystals were solubilized using 100 µl of DMSO (Sigma-Aldrich). Absorbance was measured at 570 nm in a microplate spectrophotometer (Perkin Elmer, Waltham, Massachusetts, USA). Cell viability was calculated with the following formula: cell viability = absorbance of sample / absorbance of control x 100 (n=5).

2.12. Tubulogenesis assay

For tube formation assay, HUVECs were cultured in M200 serum-free medium (Thermo Fisher) and seeded onto 48-well plates (2.5×10^4 cells/well) previously coated with growth factor-reduced matrigel (BD Biosciences, San Diego, CA, USA) in the presence of osteopontin (OPN) (25 µg/ml, R&D System), ICOS-Fc (25 µg/ml), or control medium with vascular endothelial growth factor (VEGF-α (10 ng/ml, R&D System). Tube formation was analyzed after 6 h of culture, as previously reported [23,25] (n=3).

2.13. In vivo experiments

Six to eight-week-old female C57BL6/J mice, either wild type or $ICOS^{-/-}$ (B6.129P2-$Icos^{tm1Mak}$/J; Charles River Laboratories,Wilmington, MA, USA) were injected subcutaneously (s.c.) with B16-F10 cells ($2.5x10^5$ cells/mouse), expressing high level of ICOSL [16]. When tumors were palpable, mice were treated every 4 days with an intravenous (i.v.) injection of either mouse ICOS-Fc, ICOS-Fc loaded in CDNS (CDNS/ICOS-Fc), empty CDNS (100 µg each), or the same volume of physiological solution (NaCl 0.9%) as control. The tumor size was measured every 4 days with a caliper, and mice were sacrificed after 2 weeks. When PLGA NPs were used, the experimental plan was the same, but mice were injected intraperitoneally (i.p.) with 100 µl of PLGA NP containing ICOS-Fc or empty PLGA. All mice were bred under pathogen-free conditions in the animal facility of the Department of Health Sciences and were treated in accordance with the University Ethical Committee. The study was approved by the Bioethics Committee for Animal Experimentation of the University of Piemonte Orientale and Ministero della Salute, Rome (n. 477/2016-PR).

2.14. Real-time reverse transcriptase polymerase chain reaction

The mRNA levels of IL-17A and RORc (marking Th17 cells), IL-10 and FoxP3 (marking Tregs), and IFNγ (marking Th1 cells) were evaluated in the tumor tissues by real time PCR (RT-PCR). The tumors were snap-frozen, and total RNA was then isolated using TRIzol reagent (Sigma-Aldrich). RNA was retrotranscribed using QuantiTect Reverse Transcription Kit (Qiagen, Hilden, Germany). IL-10, FoxP3, IL-17A, and RORc and IFNγ expression was evaluated through gene expression assay (Assay-on Demand, Applied Biosystems, Forest City, CA, USA). Glyceraldehyde 3-phosphate dehydrogenase (GAPDH) was used to normalize the cDNA amounts. Real Time PCR was performed using the CFX96 System (Bio-Rad Laboratories, CA, Hercules, USA) in duplicate for each sample in a 10 µl final volume containing 1 µl diluted cDNA, 5 µl TaqMan universal PCR master mix (Applied Biosystem, Foster City, CA), and 0.5 µl TaqMan Gene Expression Assays (Applied Biosystem). The thermocycler parameters were 95°C for 10 min, followed by 40 cycles of 95°C for 15 sec and 60°C for 1 min. The results were analyzed by the ΔΔCT method.

2.15. Anti-CD31 immunofluorescence

Immediately after dissection, tumor samples were embedded in OCT compound (Killik, Bioptica Milano SpA) and stored at -80°C until use. Tumor tissues were cut with a cryostat (thickness 4-5 µm) and treated with 4% paraformaldehyde (Sigma-Aldrich) diluted in PBS for 5 min at room temperature to fix the sample on the glass slides. The samples were then blocked with 5% normal goat serum (R&D System) in PBS for 1 h in order to block aspecific sites to which the primary antibody could bind. To detect CD31 expression, slides were incubated with the primary antibody rabbit anti-CD31 (Abcam, Cambridge, UK), diluted 1:50 over night at 4°C in a humid chamber. The secondary antibody used was an anti-rabbit Ig Alexa fluor 488-conjugated (Thermo-Fisher), diluted 1:400. The sections then were stained with 0.5 mg/ml of the fluorescent dye 4,6-diamidino-2-phenylindole-dihydrochloride (DAPI, Sigma-Aldrich) for 5 min to highlight cell nuclei and then mounted using prolong anti-fade mounting

medium (Slow Fade Anti FADE Kit, Molecular Probes Invitrogen). The sections were then observed by a fluorescence microscope (Leica, Italy) and analyzed by Image Pro Plus Software for micro-imaging 5.0 (Media Cybernetics, version 5.0, Bethesda, MD, USA). Tumor microvessel density (TMD) was measured by evaluating the CD31-positive area and the total tumor area *per* field upon slide scanning (Panoramic midi II, 3D Histech, Budapest, Hungary), as previously described [26,27].

2.16. Data analysis

Statistical analyses were performed using Mann-Whitney Test using GraphPad Instat Software (GraphPad Software, San Diego, CA, USA). Data are expressed as mean and standard error of the mean (SEM) and statistical significance was set at $P<0.05$.

3. Results

3.1. Characterization of ICOS-Fc-loaded CDNS

To obtain a nanoformulation suitable for ICOS delivery and administration *in vivo*, a purposely tuned manufacturing method was carried out comprising a HPH step to reduce the size of the CDNS. This allowed us to obtain an aqueous nanosuspension of CDNS with an average diameter less than 200 nm and a low polydispersity index (Table 1, Fig. 1a, b). The CDNS showed a negative surface charge with zeta potential value of about -30 mV, a value high enough to avoid aggregation phenomena (Table 1).

	Blank CDNS	**ICOS-Fc loaded CDNS**	**Blank PLGA NP**	**ICOS-Fc loaded PLGA NP**
Average diameter ± SD (nm)	160.8 ± 2.4	164.5 ± 5.6	221.9 ± 3.0	249.8 ± 5.5
Polidispersity index	0.16 ± 0.02	0.19 ± 0.03	0.27 ± 0.02	0.30 ± 0.02
Zeta potential ± SD (mV)	- 30.2 ± 4.5	- 29.4 ± 3.3	-12.03 ± 2.33	- 8.69 ± 2.06

Table 1. Physico-chemical characteristics of blank and ICOS-Fc loaded CDNS and PLGA NPs

The size and size distribution of blank and ICOS-Fc-loaded CDNS (CDNS/ICOS-Fc) formulations measured by NTA are shown in Fig. 1a.

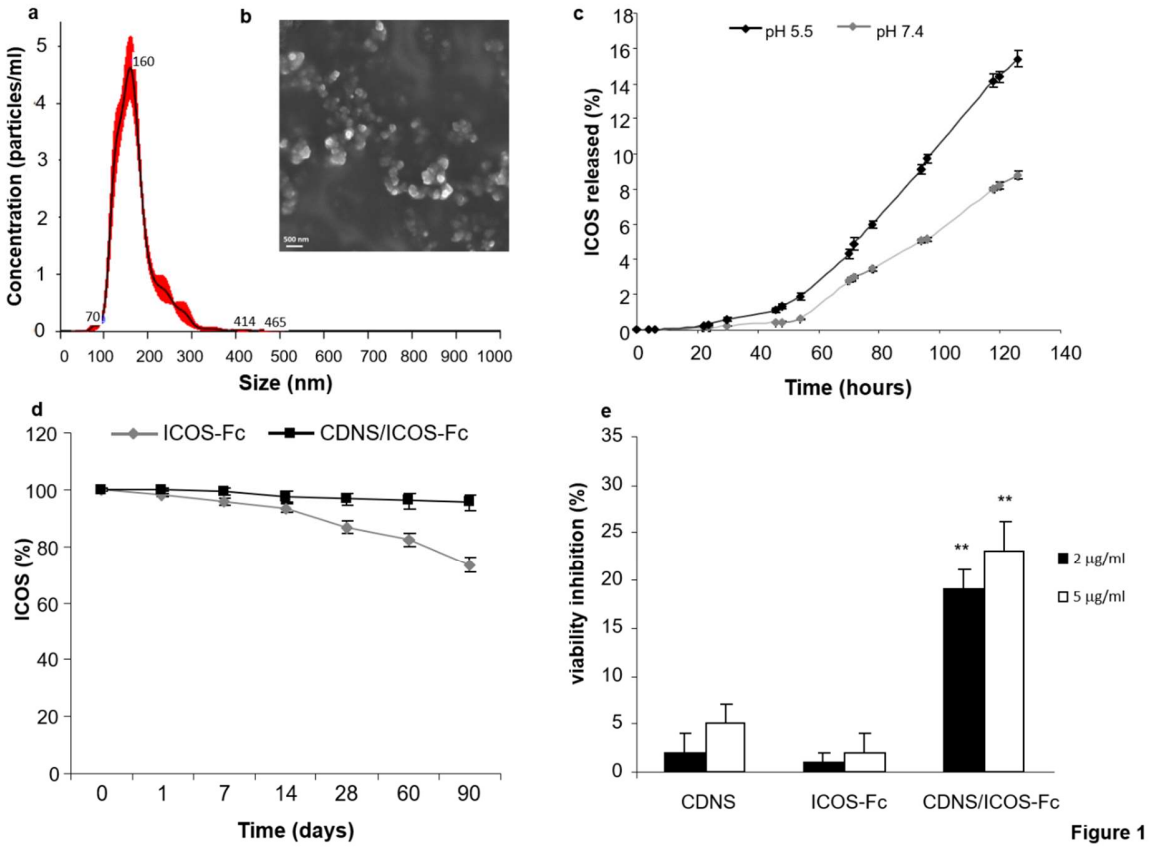

Fig. 1. Characterization of CDNS formulations. (a) CDNS size distribution was determined using NanoSight Nanoparticle Tracking Analysis (NTA). (b) Field-emission scanning electron microscopy (FESEM) image of ICOS-Fc loaded CDNS (scale bar 500 nm). (c) *In vitro* release kinetics of ICOS-Fc from ICOS-Fc loaded CDNS upon incubation at 37°C, evaluated by BCA assay. (d) *In vitro* evaluation of ICOS-Fc stability over time upon storing at 4°C, evaluated by BCA assay (n=3). (e) Effect of free ICOS-Fc (ICOS-Fc), empty CDNS (CDNS), and CDNS loaded with ICOS-Fc on viability of B16-F10 cells evaluated after a 72 hr incubation with 2 and 5 µg/ml of each drug preparation (n=5); $^{**}P<0.01$ *vs* free ICOS-Fc and empty CDNS.

ICOS-Fc was incorporated in CDNS following incubation at room temperature without the addition of any solvent, reaching an encapsulation efficiency of 91.5 % and a loading capacity of 8.5 %. No changes in CDNS physicochemical characteristics were observed after ICOS-Fc incorporation.

The *in vitro* release of ICOS-Fc from CDNS/ICOS-Fc was assessed by incubating these NPs in PBS either at pH 7.4 or 5.5 and sampling the supernatant at fixed times. The concentration of ICOS-Fc released was assessed by the BCA method (Fig. 1c). A slow and prolonged *in vitro* release kinetics of ICOS-Fc from the nanoformulation was observed. The lack of an initial burst effect confirmed the

incorporation of ICOS-Fc in the CDNS nanostructure. The *in vitro* release profile of ICOS-Fc from CDNS showed the highest correlation with the zero-order kinetic model, suggesting that ICOS-Fc is mainly released by passive diffusion through the polymer matrix. Moreover, CDNS nanoformulation showed a pH-sensitive release profile, with an increased cumulative release at pH = 5.5.

CDNS/ICOS-Fc were chemically and physically stable up to 6 months stored at 4 °C, thereby protecting ICOS-Fc from degradation (Fig. 1d). ICOS-Fc activity was measured over time by assessing its ability to stain $ICOSL^+$ cell lines, thus confirming the functional stability of the molecule (data not shown). In addition, the stability of the nanoformulation was investigated at 25 °C and at physiological temperature (37 °C). No significant changes in the physico-chemical parameters of CDNS/ICOS-Fc and no aggregation phenomena were observed after 48 h of incubation at 25 °C and 37 °C (data not shown). In addition, the ICOS-Fc concentration in the CDNS/ICOS-Fc did not change after 48 h (99.86 % of the initial ICOS-Fc content), confirming the CDNS/ICOS-Fc stability.

Cell toxicity of the CDNS formulations was assessed by performing MTT assay on B16-F10 cells incubated with titrated amounts (0.5, 1, 2, 5 μg/ml) of empty or CDNS/ICOS-Fc. B16-F10 cells treated with CDNS/ICOS-Fc, but not with empty CDNS, produced a 30% inhibition of cell viability only at the highest doses (2 and 5 μg/ml) (Fig.1e), whereas no effect was detected at the 0.5 and 1 μg/ml doses (data not shown).

3.2. CDNS/ICOS-Fc inhibits tumor growth in vivo.

To determine CDNS antitumor activity *in vivo*, C57BL6/J mice carrying palpable subcutaneous B16-F10 tumors were treated by i.v. injection with either free ICOS-Fc, CDNS/ICOS-Fc, empty CDNS (100 μg in 100 μl each), or the same volume of saline every 4 days, and tumor growth was monitored at T0, when the tumor was palpable, and every 4 days afterward (T1, T2, and T3). As shown in Fig. 2, CDNS/ICOS-Fc substantially inhibited tumor growth, whereas free ICOS-Fc and empty CDNS had no

significant effect. Analysis of tumor infiltrating lymphocytes by immunofluorescence and flow cytometry did not detect significant differences in the percentages of $CD4^+$ or $CD8^+$ T cells or $CD4^+CD25^+FoxP3^+$ Treg cells in mice receiving different treatments. The ratios between $CD8^+$ T cells and Treg cells were similar in the different groups and were 3.9±1.5 (PBS treatment), 4±0.8 (CDNS), 5.5±3 (free ICOS-Fc), 3±1.8 (CDNS/ICOS-Fc).

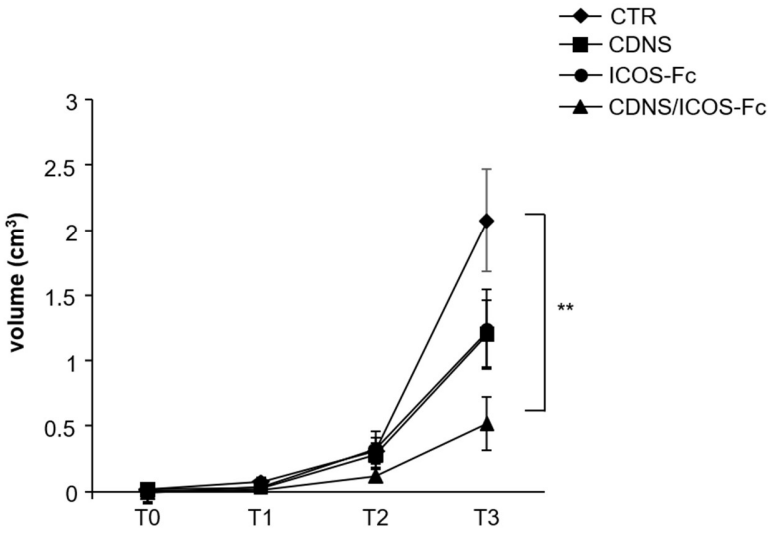

Fig. 2. Effect of different formulations of ICOS-Fc on the growth of B16-F10 tumors in C57BL6/J wild-type mice. C57BL6/J wild-type mice with palpable subcutaneous B16-F10 tumors were treated every 4 days with saline (CTR, black diamonds), CDNS alone (black squares), ICOS-Fc (black circles) or CDNS loaded with ICOS-Fc (black triangles). Tumor volume (cm^3) was evaluated every four days after the first treatment (T0, when the tumor was palpable). Each treatment involved 5 mice *per* experiment (**$P \leq 0.01$ *vs* control values).

Next, we sought to determine the mechanisms underlying CDNS/ICOS-Fc anti-tumor activity. To this end, we treated C57BL6/J mice carrying subcutaneous B16-F10 tumors with CDNS/ICOS-Fc empty CDNS, or saline as described above and assessed the extent of tumor infiltration (Treg and Th17 cell markers) and vascularization in T3 tumors. As expected, CDNS/ICOS-Fc treatment inhibited B16-F10 tumor growth, while saline solution or empty CDNS injection had no effect (Fig. 3a).

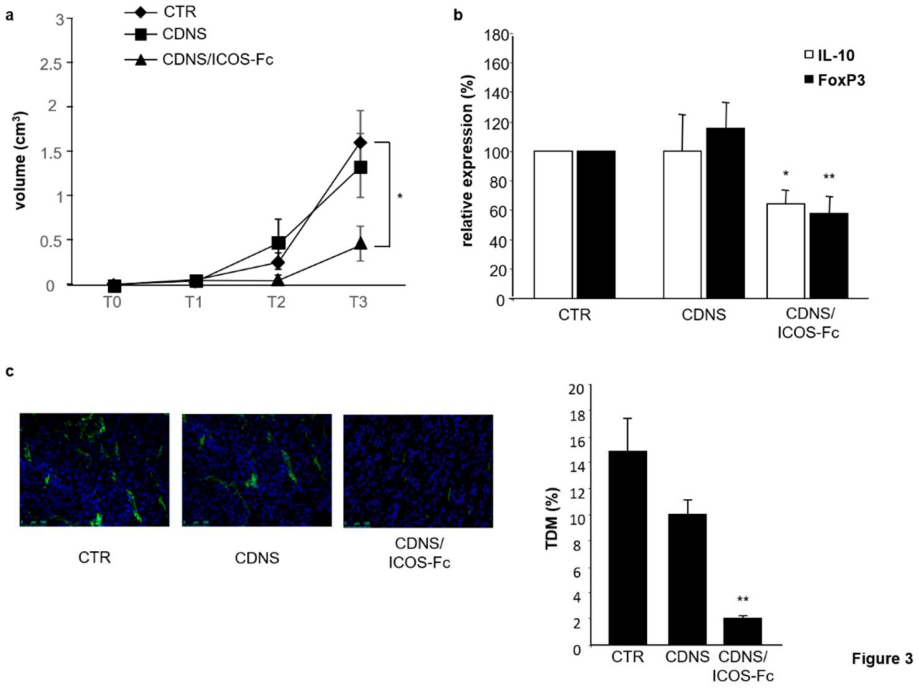

Fig. 3. Effect of CDNS-ICOS-Fc on B16-F10 tumor growth on Treg markers *ex vivo* and angiogenesis *in vivo* (a) C57BL6/J wild-type mice with palpable subcutaneous B16-F10 tumors were treated and analyzed as described in the legend to fig. 2. Saline (CTR, black diamonds), CDNS alone (black squares), and CDNS loaded with ICOS-Fc (black triangles). Each treatment involved 5 mice/experiment. (b) Expression levels of IL-10 and FoxP3, were evaluated by RT-PCR in lysates from tumor masses. The data are normalized for the expression of each gene in control mice (set at 100%); (n=5). (c) Immunofluorescence staining for anti-CD31 of tumors tissue sections from mice treated with saline (CTR), CDNS alone or CDNS loaded with ICOS-Fc. The slides were stained with a rabbit α-mouse CD31 Ab plus a secondary α-rabbit antibody conjugated with Alexa Fluor® 488. Microphotographs of CD31 staining from a representative experiment (green; magnification 200x). Graph shows tumor microvessel density (TMD) determined as the percentage of CD31-positive area on the tumor sections. Three randomly selected areas from three tumors from each group were analyzed. (*P<0.05, **$P\leq$ 0.01 *vs* control values).

Expression of Treg and Th17 cell markers was assessed by measuring mRNA levels of IL-10/FoxP3, marking Treg cells, and IL-17/RORc, marking Th17 cells, by RT-PCR. Mice treated with CDNS/ICOS-Fc displayed significantly lower FoxP3 and IL-10 expression levels compared to saline solution or empty CDNS-treated mice (Fig.3b). By contrast, RORc expression was similar in all groups, while IL-17 expression was undetectable (data not shown). The analysis was then extended to the IFNγ mRNA, marking Th1 cells, cytotoxic T cells and NK cells, but its expression was similar in all groups (data not shown); the IFNγ/IL-10 ratios were 1.2±0.2 (PBS), 2±0.6 (CDNS), 2.5±0.5 (CDNS/ICOS-Fc)

with a trend of increasing between PBS and CDNS/ICOS-Fc (p=0.09). The extent of tumor vascularization was determined by staining tumor sections with a fluorescent anti-CD31 antibody. In addition, tumor microvessel density (TMD) was evaluated by measuring the CD31-positive area by automatic digital scanning. Results showed that vascular CD31 expression levels were lower in the CDNS/ICOS-Fc-treated mice than those observed in saline- or CDNS-treated mice (Fig.3c).

We then assessed CDNS/ICOS-Fc-mediated anti-tumor activity in ICOS-deficient mice carrying B16-F10 tumors. Interestingly, treatment with CDNS/ICOS-Fc significantly inhibited B16-F10 tumor growth also in these ICOS-deficient mice (Fig.4a).

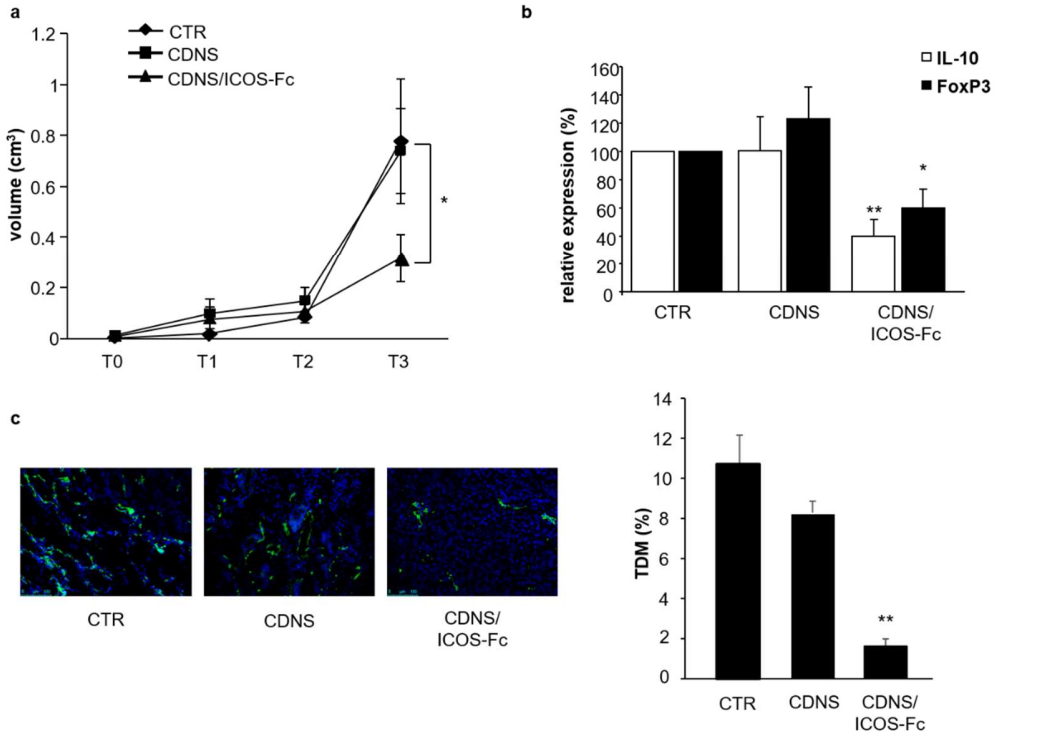

Figure 4

Fig. 4. Effect of ICOS-Fc on the growth of B16-F10 tumors in ICOS-deficient mice. Mice with palpable subcutaneous B16-F10 tumors were treated every 4 days with saline (CTR, black diamonds), CDNS alone (black squares) or CDNS loaded with ICOS-Fc (black triangles). (a) Tumor volumes (cm^3) were evaluated every four days after the first treatment performed at T0 (i.e. when the tumor was palpable); each group involved 8 mice. (b) Expression of IL-10 and FoxP3 mRNA levels in tumor lysates measured by RT-PCR; values are normalized for basal expression in the control group set at 100%. (c) Microphotographs of CD31 staining from a representative experiment (green, magnification 200x); the graph shows the TMD determined as the percentage of CD31-positive area calculated as described in the legend to Fig.3c. (*P<0.05, **P≤0.01 *vs* control values).

Furthermore, CDNS/ICOS-Fc treatment led to downmodulation of IL-10 and FoxP3, as measured by RT-PCR and vascular CD31 in the tumor mass, as judged by immunofluorescence (Fig.4b and 4c). Expression of the IL-17, RORc, and IFNγ mRNA was similar in all groups (data not shown); the IFNγ/IL-10 ratios were 1.1±0.3 (PBS), 4.9±1.7 (CDNS), 6.4±2 (CDNS/ICOS-Fc) with a significant difference between PBS and CDNS/ICOS-Fc ($p=0.016$).

3.3. Anticancer activity of PLGA/ICOS-Fc nanocarriers

To assess whether ICOS-Fc would also exert anticancer activity when loaded into other types of biocompatible/biodegradable NPs, we injected i.p. ICOS-Fc loaded in PLGA NPs (PLGA/ICOS-Fc) in B16-F10 bearing wild type mice.

Physico-chemical characterization of PLGA NPs was performed as for CDNS. Results showed that PLGA NPs displayed an average diameter of about 250 nm, a low polydispersity index, and a negative surface charge with zeta potential value of about -10 mV (Table 1, Fig. 5a, b).

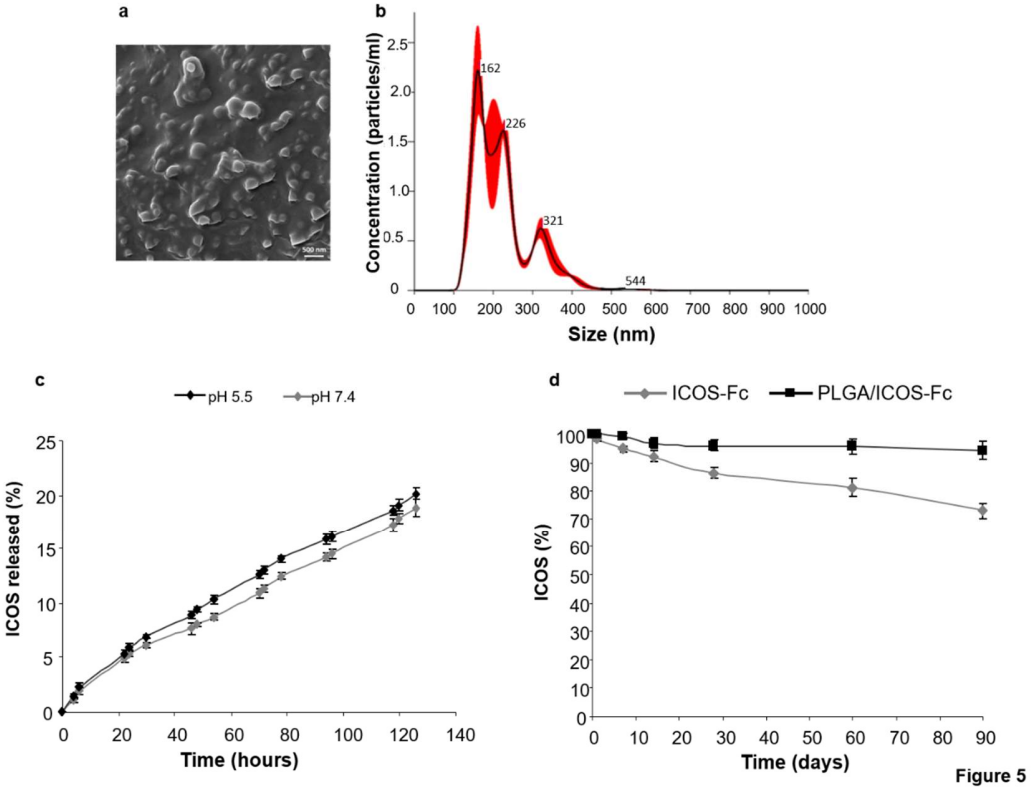

Fig. 5. Characterization of PLGA NP formulations. (a) Field-emission scanning electron microscopy (FESEM) image of ICOS-Fc loaded PLGA NPs (scale bar 500 nm). (b) PLGA NP size distribution determined using NanoSight Nanoparticle Tracking Analysis (NTA). (c) *In vitro* release kinetics of ICOS-Fc from ICOS-Fc loaded PLGA NPs upon incubation at 37°C, evaluated by BCA assay. (d) *In vitro* evaluation of ICOS-Fc stability over time upon storing at 4°C, evaluated by BCA assay (n=3).

ICOS-Fc incorporation reached an encapsulation efficiency of 96.8 % and a loading capacity of 1.1 %. No changes in physico-chemical characteristics were observed after ICOS-Fc incorporation. Analysis of the *in vitro* release of ICOS-Fc from PLGA NPs showed a slow and prolonged *in vitro* release kinetics without an initial burst effect and similar at pH 7.4 and 5.5 (Fig. 5c). PLGA/ICOS-Fc nanoformulations were chemically and physically stable up to 6 months stored at 4° C (Fig. 5d). On the contrary, aggregation phenomena occurred after 48 h of incubation at 37 °C, increasing the particle size

(data not shown). Cell toxicity of the PLGA NPs was assessed by MTT assay on B16-F10 cells incubated with titrated amounts (0.5, 1, 2, 5 μg/ml) of empty PLGA or PLGA/ICOS-Fc. In good agreement with the results obtained with CDNS, we observed 30% inhibition of cell viability by PLGA/ICOS-Fc, but not empty PLGA, only at the highest doses (2 and 5 μg/ml) but not at the 1 and 0.5 μg/ml doses (data not shown).

To determine NP antitumor activity *in vivo*, C57BL6/J mice carrying palpable subcutaneous B16-F10 tumors were treated with PLGA/ICOS-Fc, empty PLGA, or saline solution every 4 days, and tumor growth was monitored at T0, when the tumor was palpable, and every 4 days afterward (T1, T2, and T3). Results showed that treatment with PLGA/ICOS-Fc effectively inhibited the growth of B16-F10 tumors compared to both control treatments (Fig.6a), and decreased expression of vascular CD31 in the tumor mass, as detected by immunofluorescence (Fig.6b).

In contrast to what observed in wild type CDNS/ICOS-Fc-treated mice, expression levels of the IL-10 and FoxP3 mRNA were not significantly inhibited by PLGA/ICOS-Fc (Fig. 6c). Expression of the IL17, RORc, and IFNγ mRNA was similar in all groups (data not shown); the IFNγ/IL-10 ratios were 1.2±0.3 (PBS), 0.8±0.2 (PLGA), 1.6±0.4 (PLGA/ICOS-Fc) with a significant difference between PLGA and PLGA/ICOS-Fc ($p=0.04$).

Since PLGA nanoparticles are capable of sustained release of the encapsulated drug [28], we assessed the effect of single dose of PLGA/ICOS-Fc delivered at T=0, when the tumor was palpable. Results showed that, also in this case, treatment with PLGA/ICOS-Fc effectively inhibited the growth of B16-F10 tumors compared to both control treatments (Fig.6d), and decreased expression of vascular CD31 in the tumor mass, as detected by immunofluorescence (data not shown), without significant effects on expression of the IL-10, FoxP3, IL-17, RORc, and IFNγ mRNA (data not shown); the IFNγ/IL-10 ratios were 1.4±0.4 (PBS), 2.1±0.5 (PLGA), 1.7±0.7 (PLGA/ICOS-Fc) without significant differences between the groups.

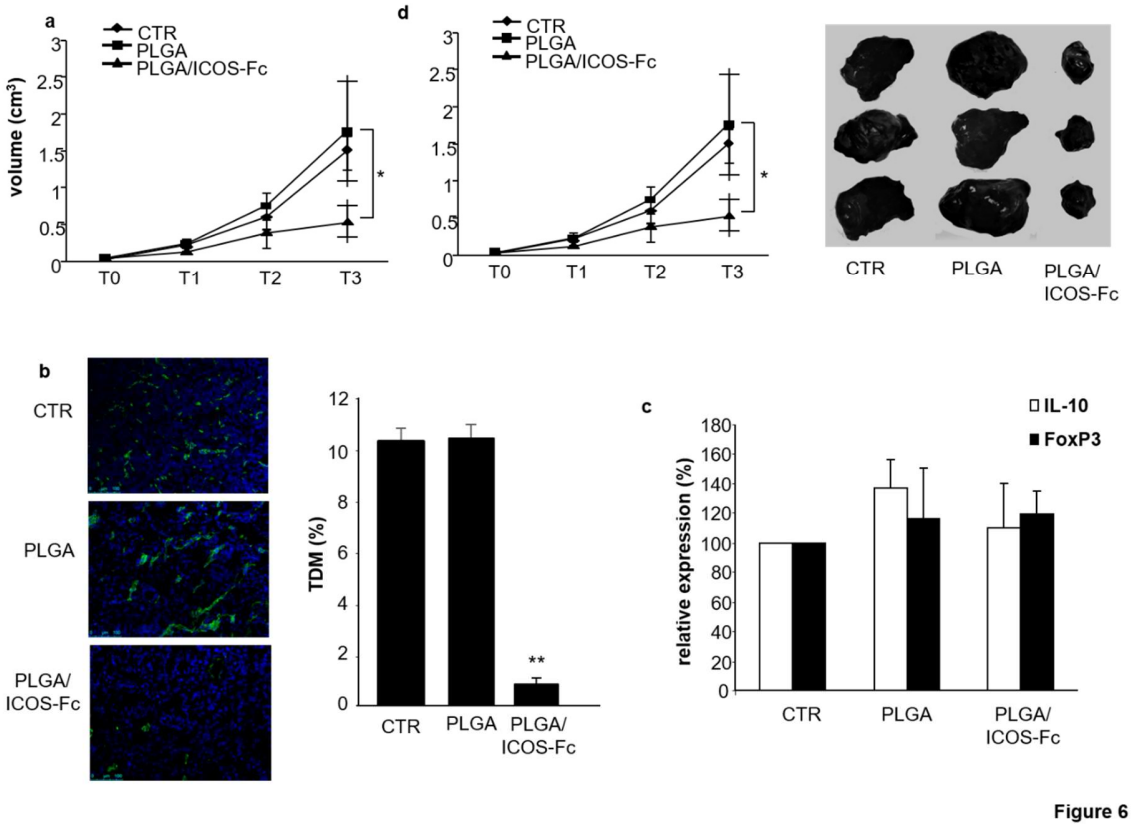

Fig. 6. Effect of ICOS-Fc encapsulated on PLGA on the growth of B16-F10 tumors in C57BL6/J wild-type mice. (a-c) Mice with palpable subcutaneous B16-F10 tumors were treated every 4 days with saline (CTR, black diamonds), PLGA alone (black squares) or PLGA loaded with ICOS-Fc (black triangles). (a) Graph shows the tumor volume curves (cm^3); tumors were evaluated every four days after the first treatment performed at T0 (i.e. when the tumor was palpable); each treatment involved 8 mice. (b) Microphotographs of CD31 staining from a representative experiment (green; magnification 200x); the graph shows TMD determined as the percentage of CD31-positive area calculated as described in the legend to Fig. 3c. (c) Expression of IL-10 and FoxP3 in tumor lysates analyzed by RT-PCR; values are normalized for the expression in the control group set at 100%. (d) Mice with palpable subcutaneous B16-F10 tumors were treated with a single dose of each treatment at T0; graph shows the tumor volume curves (cm^3) evaluated as in (a); each treatment involved 8 mice; photographs show representative tumors. (*P<0.05, **P≤0.01, from the respective control values).

3.4. ICOS-Fc inhibits EC tubulogenesis in vitro

Inhibition of tumor vascularization by CDNS/ICOS-Fc implied that ICOS-Fc inhibits tumor angiogenesis *in vivo*, which would be consistent with previous data showing that ICOS-Fc inhibits adhesiveness and migration of human umbilical vascular cells (HUVECs) [15,16]. However, previous experiments showed that ICOS-Fc had no effect on HUVEC tubulogenesis induced by VEGF-α, which is an *in vitro* measure of angiogenesis. Thus, we assessed the effect of free human ICOS-Fc on HUVEC tubulogenesis induced by osteopontin (OPN), which is an angiogenetic factor produced by several tumors [29]. As shown in Fig. 7a and b, ICOS-Fc substantially inhibited OPN-induced tubulogenesis, whereas as expected ICOS-Fc failed to inhibit VEGF-α-induced tubulogenesis.

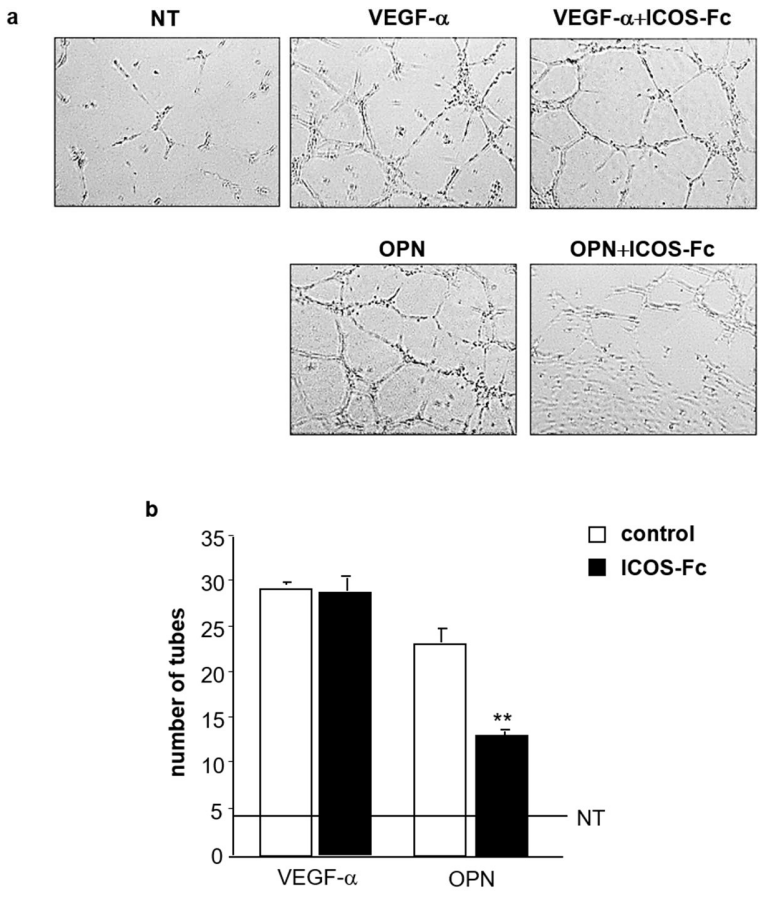

Figure 7

Fig. 7. Effect of ICOS-Fc on HUVEC tubulogenesis *in vitro*. For tube formation assay, HUVECs were treated, maintained, and cultured in the presence or absence of OPN (25 μg/ml) or VEGF-α (10 ng/ml) with or without ICOS-Fc (25 μg/ml), as indicated. The morphology of capillary-like structures formed by HUVECs was analyzed 6 h after culturing using an inverted microscope. (a) Panels show a representative tubulogenesis experiment photographed with a digital camera (magnification 10x). (b) The results are expressed as number of tubes *per* three wells cultured in each condition (n=3) (**$P \leq 0.01$ *vs* control values). The horizontal line (NT) shows tube formation of HUVEC in the absence of the angiogenic stimuli.

4. Discussion

Cyclodextrin based nanosponges (CDNS), a class of biodegradable and biocompatible cross-linked polymer nanoparticles, have been recently attracted much research in the field of anticancer drug delivery to enhance their properties and modulate their release. [30,31]. A recent European Union report indicates that CDNSs are a promising innovative system to be developed for therapeutic clinical applications. Indeed, previous *in vitro* and *in vivo* experiments showed the ability of this type of nanosponges to enhance anticancer drug delivery to the tumor site, increasing remarkably the therapeutic effectiveness and decreasing adverse side effects. [32-34]. Many anticancer small molecules have been incorporated in the nanosponge structure, such as camptothecin, paclitaxel, doxorubicin, 5-fluoruracile, curcumin, resveratrol, temozolamide, erlotinib [26,32,34-41]. In addition, CDNS showed the ability to store and protect macromolecules, such as peptides and proteins. Finally, Shende *et al.* carried out *in vivo* acute and repeated dose toxicity studies on rats, demonstrating the safety of CDNS [42].

Here, we show that ICOS-Fc encapsulated in CDNS can effectively inhibit the growth of established B16-F10 melanomas through two combined mechanisms leading to decreased of tumor vascularization and enhanced anticancer immune response. This is intriguing since therapeutic combination regimens, that exploit synergic effects of active molecules with different mechanism to fight tumor cells, is one of the advanced therapeutic [43,44]. In particular, combinatorial immunostimulatory nanomedicines have been proposed as promising tools to elicit antitumor immunity and improve the response [45-48]. Moreover, Conniot *et al.* reported that the combination of different immunotherapeutic approaches, such as mannosylated nanovaccines to activate dendritic cells, immune checkpoint modulators acting on cytotoxic T cells, and ibrutinib inhibiting the myeloid-derived suppressor cells, elicit specific immune response and strong inhibition of two murine models of melanoma growth [49]. However, cyclodextrin-based nanosponges have not been previously studied as nanocarriers for immunotherapy compounds.

In previous researches, ICOSL triggering by ICOS-Fc solution showed to inhibit migration and adhesion of DCs, ECs, and several tumor cell lines *in vitro* [15,17]. Moreover, free ICOS-Fc as such prevented lung metastatization of $ICOSL^+$ tumor cells by acting on both tumor and host cells, with the latter possibly being ECs. Indeed, after injecting human $ICOSL^+$ tumor cells in the tail vein of immunodeficient mice, we could achieve maximum inhibition of metastasis only by treating mice with both human and mouse ICOS-Fc, which are species-specific. To explain this behavior, one possibility is that human ICOS-Fc inhibits the adhesiveness and migration of the human tumor cells, whereas mouse ICOS-Fc impairs the adhesiveness of vascular ECs in the mouse environment [16].

By contrast, we have consistently failed to inhibit the growth of transplantable and spontaneous tumors in several mouse models by administering free ICOS-Fc in solution (unpublished data).

In light of these data, we asked whether the loading of ICOS-Fc into nanosponges would allow to obtain inhibition of tumor growth taking into account the nanocarrier capability to magnify anticancer drug delivery. Moreover, we also prepared ICOS-loaded PLGA nanoparticles, for comparison purpose. PLGA is a biocompatible and biodegradable polymer approved by Food and Drug Administration (FDA) and European Medicine Agency (EMA) for parenteral administration [50]. Many PLGA nanodelivery system have been studied for anticancer drug and protein delivery showing their effectiveness [51].

It is worth noting that nanocarriers, thanks to their nanoscale size, can accumulate in tumor tissues for the Enhanced Permeation and Retention (EPR) effect, which enables these nanoformulations to cross efficiently the wide fenestrations of the tumor neovessels and accumulate into the tumor mass [30,31].

Through this nanocarrier-based therapeutic approach, we were able to achieve significant anticancer activity using the two types of ICOS-Fc nanoformulations (i.e. CDNS and PLGA NPs) also if each is characterized by distinctive size, physicochemical properties and *in vitro* release kinetics.

CDNS showed smaller size than PLGA NP, which allowed their intravenous administration. As far as concern the *in vitro* release, both nanocarriers showed sustained release kinetics. In particular, CDNS

have a pH- sensitive release behavior, since the release kinetics is faster at pH = 5.5 than at pH = 7.4. This is related to the presence of free ionizable carboxylic groups in the nanosponge polymer matrix. Such ionizable weak acid groups can be protonated or deprotonated according to external pH value, affecting the chemical structure of CDNS. Indeed, they are partly dissociated at mild acidic pH values (5.5), determining the electrostatic repulsion of negative charged carboxylic groups and consequently an enlargement of CDNS matrix. Interestingly, pH= 5.5 is the value present in the endosomes and the tumor microenvironment is more acidic than the blood compartment. This behavior may be an advantage for the delivery to the tumor site, making CDNS an environment-sensitive drug delivery system.

The two types of nanocarriers employed in our study were injected into the mice by different administration routes. CDNS/ICOS-Fc were injected intravenously because preliminary experiments had not shown any anticancer activity upon intraperitoneal injection, probably due to rapid clearance of CDNS by peritoneal macrophages (data not shown). By contrast, PLGA/ICOS-Fc was effective when delivered intraperitoneally, which was then chosen as the preferred administration route. Moreover, CDNS sizes did not change after incubation at 37 °C, while PLGA NPs underwent aggregation phenomena.

Another interesting delivery difference between free and NP-encapsulated ICOS-Fc is that the latter can be internalized by cells [28, 32-34]. Indeed, different types of NPs have been used to increase tumor cell internalization of several antineoplastic chemotherapeutic agents, exploiting the NP capability to be taken up by the cells. Previous studies showed that fluorescent –labelled CDNS can be easily and fast internalized in various cell lines [26,33,34]. This feature may be relevant also for ICOS-Fc since ICOSL can be expressed independently on either the cell surface and intracellularly [52]. For instance, ICOSL expression has been detected both on the surface and in the cytoplasm of regenerating and degenerating muscle fibers [53]. Moreover, we found that several tumor cell lines, including melanoma cell lines, may independently express ICOSL on the cell surface and intracellularly (data not shown).

Intriguingly, the role of cytoplasmic ICOSL is not known, but it is possible that binding of ICOS-Fc to intracellular ICOSL either blocks ICOSL stocks available for surface expression or alters unknown functions of intracellular ICOSL.

Overall, our findings indicate that the antitumor activity of NP-loaded ICOS-Fc relies on at least three distinct mechanisms.

First, immunomodulation, as shown by decreased expression of IL-10 and FoxP3 in the tumor mass from mice treated with CDNS/ICOS-Fc, with an increasing trend of the IFNγ/IL-10 ratio. This observation suggests that CDNS/ICOS-Fc have the capability to inhibit Tregs, known to suppress the anti-tumor effector immune response, which is an effect similar to that displayed by immune checkpoint inhibitors, such as the antagonists of the CTLA-4 and PD-1/PD-L1 systems. This effect might be due to ICOS-Fc-mediated inhibition of the interaction between ICOS expressed on T-cell surface and ICOSL expressed on the surface of several cell types, including tumor cells. This is in line with previous reports showing that treatment with blocking mAb against either ICOS or ICOSL inhibits the development of Tregs and potentiates the anti-tumor immune response in mouse experimental tumors [54-57]. Moreover, cyclodextrin based systems have been proposed for cancer immunotherapy. Xu *et al*. used the cyclodextrin complexation strategy to formulate NGS919, a small immunotherapeutic drug, for injection in combination with paclitaxel [58]. Recently, a polymeric nanolipogel has been developed for the co-delivery of IL-2 and TGF-β. The nanosystem consisted of biodegradable polymers encapsulating cytokines and drug cyclodextrin complex to obtain a sustained release in the tumor microenvironment. An enhanced antitumor immunoresponse was observed in the B16/B2 mouse melanoma model [59].

It must be noted that, in our model, the decrease in IL-10 and FoxP3 expression levels and increased IFNγ/IL-10 ratio were also detected in ICOS-deficient mice, thereby suggesting that mechanisms different from blockade of the endogenous ICOS/ICOSL interaction may be involved. For instance, a

role might be played by functional effects of ICOSL triggering on antigen presenting cells involved in T cell activation. Surprisingly, this immune modulation was inconsistent in PLGA/ICOS-Fc-treated mice despite the effective anti-tumor activity of this formulation, which indicates that this might not be a primary mechanism. The differences in immunomodulatory activity of CDNS/ICOS-Fc *vs* PLGA/ICOS-Fc might be ascribed to the different delivery routes used (i.v. *vs* i.p., respectively) or to the different release kinetics of ICOS-Fc from the two nanoformulations *in vivo*. However, we cannot rule out that differences in biodistribution within the secondary lymphoid tissue or differential interaction with specific immune cell types may also affect the immunomodulatory properties of these nanoparticles and free ICOS-Fc.

Second, inhibition of tumor angiogenesis, as shown by decreased tumor vascularization in CDNS/ICOS-Fc- or PLGA/ICOS-Fc-treated mice. This effect was also detected in ICOS-deficient mice, indicating that it is independent of the inhibition of endogenous ICOS/ICOSL interaction. Fittingly, ICOS-Fc was found to inhibit HUVEC tubulogenesis induced *in vitro* by OPN, a pro-angiogenetic factor produced by several cell types in the tumor microenvironment, including tumor cells [29]. By contrast, ICOS-Fc failed to inhibit VEGF-α induced tubulogenesis. This discrepancy could be partly explained by qualitative, rather than quantitative, differences between the two stimuli since ICOS-Fc was ineffective even at low VEGF-α concentrations (data not shown) and recent data show that ICOS, ICOSL and OPN are involved in a unique molecular network playing a role in several cell functions (Ranieri et al, manuscript submitted).

Third, NP-loaded ICOS-Fc might directly exert inhibitory effects on adhesion, migration, and endothelial mesenchymal transition of the tumor cells expressing ICOSL, as suggested by our *in vitro* data [16]. Interestingly, NP-loaded ICOS-Fc may also exert an inhibitory effect on tumor cell growth as shown by MTT analysis of B16-F10 cells *in vitro* (Fig. 1e). Intriguingly, this effect was not detected

using free ICOS-Fc, confirming previous data in other cell lines [16]. One possibility may be due to the ability of our nanoformulations to increase ICOS-Fc cell internalization, which would in turn enhance the interaction of ICOS-Fc with intracellular ICOSL whose function is not known to date. Alternatively, ICOS-Fc exposed on the surface of the NPs might increase crosslinking of ICOSL expressed on the cell surface, potentiating its signaling.

5. Conclusion

In conclusion, our data indicate that, upon encapsulation in nanoparticles, ICOS-Fc behaves as an effective antitumor agent by triggering an anticancer immune response, inhibiting tumor angiogenesis, and possibly altering the behavior of the tumor cells.

Here, we indirectly confirmed the ability of ICOS-Fc to inhibit tumor metastatization, which may further contribute to the anti-neoplastic effect of this compound. Although further clarification of this issue was beyond the scope of the present work due to the low and inconsistent rate of spontaneous metastatic dissemination of this B16-F10 model, preliminary data using a different tumor model seem to indicate that mice treated with encapsulated ICOS-Fc display a substantial reduction in spontaneous metastases.

Taken together, these findings indicate that ICOS-Fc has the potential to become a novel tool for combined cancer therapies because of its multi-pronged anticancer activity targeting essential steps of tumor growth.

Author contributions

D.U., D.C., C.R., conceived and designed the experiments; C.N., B.G., G-C.L., R.D., F.B., C.G. and A.M. performed the experiments; B.G., C.N., G-C.L., and A.M. performed data analysis, A.C., T.F., C.F., J-M. R., Y.J, C-M.T., G.M, and R.F. provided technical support and corrections to the manuscript; D.U., D.C., and C.R., wrote the manuscript.

Competing financial interests

A patent application has been submitted for use of ligands of ICOSL loaded in nanoparticles in tumors treatment.

Funding

This work was supported by the Associazione Italiana Ricerca sul Cancro (IG 20714, AIRC, Milano), Fondazione Amici di Jean (Torino), and Fondazione Cariplo (2017-0535).

References

[1] V. Redoglia, U. Dianzani, J.M. Rojo, P. Portolés, M. Bragardo, H. Wolff, D. Buonfiglio, S. Bonissoni, C.A. Jr. Janeway, Characterization of H4: a mouse T lymphocyte activation molecule functionally associated with the CD3/T cell receptor, Eur. J. Immunol. 26 (11) (1996) 2781-2789. DOI: 10.1002/eji.1830261134

[2] D. Buonfiglio, M. Bragardo, S. Bonissoni, V. Redoglia, R. Cauda, S. Zupo, V.L. Burgio, H. Wolff, K. Franssila, G. Gaidano, A. Carbone, C.A. Jr Janeway, U. Dianzani, Characterization of a novel human surface molecule selectively expressed by mature thymocytes, activated T cells and subsets of T cell lymphomas, Eur. J. Immunol. 29 (9) (1999) 2863-2874. DOI: 10.1002/(SICI)1521-4141(199909)29:09<2863::AID-IMMU2863>3.0.CO;2-W

[3] A.Hutloff, , A.M. Dittrich, K.C. Beier, B. Eljaschewitsch, R. Kraft, I. Anagnostopoulos, R. Kroczek, ICOS is an inducible T cell co-stimulator structurally and functionally related to CD28, Nature 397 (6716) (1999) 263-266. DOI: 10.1038/16717

[4] D. Buonfiglio, M. Bragardo, V. Redoglia, R. Vaschetto, F. Bottarel, S. Bonissoni, T. Bensi, C. Mezzatesta, C.A. Janeway, U. Dianzani, The T cell activation molecule H4 and the CD28-like molecule ICOS are identical, Eur. J. Immunol. 30 (12) (2000) 3463-3467. DOI: 10.1002/1521-4141(2000012)30:12<3463::AID-IMMU3463>3.0.CO;2-5

[5] M. Hedl, A. Lahiri, K. Ning, J.H. Cho, C. Abraham, Pattern recognition receptor signaling in human dendritic cells is enhanced by ICOS ligand and modulated by the Crohn's disease ICOSLG risk allele, Immunity 40 (5) (2014) 734-746. DOI: 10.1016/j.immuni.2014.04.011

[6] A.H. Sharpe, G.J. Freeman, The B7-CD28 superfamily, Nat. Rev. Immunol. 2 (2) (2002) 116-126. DOI: 10.1038/nri727

[7] R.I. Nurieva, Regulation of immune and autoimmune responses by ICOS-B7h interaction, Clin. Immunol. 115 (1) (2005) 19-25. DOI: 10.1016/j.clim.2005.02.010

[8] A.T. Bauquet, H. Jin, A.M. Paterson, M. Mitsdoerffer, I.C. Ho, A.H. Sharpe, V.K. Kuchroo, The costimulatory molecule ICOS regulates the expression of c-Maf and IL-21 in the development of follicular T helper cells and TH-17 cells, Nat. Immunol. 10 (2) (2009) 167-175. DOI: 10.1038/ni.1690.

[9] P.F. Yong, U. Salzer, B. Grimbacher, The role of costimulation in antibody deficiencies: ICOS and common variable immunodeficiency, Immunol. Rev. 229 (1) (2009) 101-113. DOI: 10.1111/j.1600-065X.2009.00764.x.

[10] R. Mesturini, S. Nicola, A. Chiocchetti, I.S. Bernardone, L. Castelli, T. Bensi, M. Ferretti, C. Comi, C. Dong, J.M. Rojo, J. Yagi, U. Dianzani, ICOS cooperates with CD28, IL-2, and IFN-gamma and modulates activation of human naïve CD4+ T cells, Eur. J. Immunol. 36 (10) (2006) 2601-2612. DOI: 10.1002/eji.200535571.

[11] R. Mesturini, C.L. Gigliotti, E. Orilieri, G. Cappellano, M.F. Soluri, E. Boggio, A. Woldetsadik, C. Dianzani, D. Sblattero, A. Chiocchetti, J. Yagi, J.M. Rojo, U. Dianzani, Differential induction of IL-17, IL-10, and IL-9 in human T helper cells by B7h and B7.1, Cytokine 64 (1) (2013) 322-330.
DOI: 10.1016/j.cyto.2013.05.021

[12] T. Fu, Q. He, P. Sharma, The ICOS/ICOSL pathway is required for optimal antitumor responses mediated by anti-CTLA-4 therapy, Cancer. Res. 71 (16) (2011) 5445-5454. DOI: 10.1158/0008-5472.CAN-11-1138.

[13] Y. Zhang Y. Luo, S.L. Qin, Y.F. Mu, Y. Qi, M.H. Yu, M. Zhong, The clinical impact of ICOS signal in colorectal cancer patients, Oncoimmunology 5 (5) (2016) e1141857. DOI: 10.1080/2162402X.2016.1141857.

[14] G. Tang, Q. Qin, P. Zhang, G. Wang, M. Liu, Q. Ding, Y. Qin, Q. Shen, Reverse signaling using an inducible costimulator to enhance immunogenic function of dendritic cells, Cell. Mol. Life Sci. 66 (18) (2009) 3067-3080. DOI: 10.1007/s00018-009-0090-7.

[15] C. Dianzani, R. Minelli, R. Mesturini, A. Chiocchetti, G. Barrera, S. Boscolo, C. Sarasso, C.L. Gigliotti, D. Sblattero, J. Yagi, J.M. Rojo, R. Fantozzi, U. Dianzani, B7h triggering inhibits umbilical vascular endothelial cell adhesiveness to tumor cell lines and polymorphonuclear cells, J. Immunol. 185 (7) (2010) 3970-3979. DOI: 10.4049/jimmunol.0903269

[16] C. Dianzani, R. Minelli, C.L. Gigliotti, S. Occhipinti, M. Giovarelli, L. Conti, E. Boggio, Y. Shivakumar, G. Baldanzi, V. Malacarne, E. Orilieri, G. Cappellano, R. Fantozzi, D. Sblattero, J. Yagi, J.M. Rojo, A. Chiocchetti, U. Dianzani, B7h triggering inhibits the migration of tumor cell lines, J. Immunol. 192 (10) (2014) 4921-4931. DOI: 10.4049/jimmunol.1300587.

[17] S. Occhipinti, C. Dianzani, A. Chiocchetti, E. Boggio, N. Clemente, C.L. Gigliotti, M.F. Soluri, R. Minelli, R. Fantozzi, J. Yagi, J.M. Rojo, D. Sblattero, M. Giovarelli, U. Dianzani, Triggering of B7h by the inducible costimulator modulates maturation and migration of monocyte-derived dendritic cells, J. Immunol. 190 (3) (2013) 1125-1134. DOI: 10.4049/jimmunol.1201816.

[18] C.L. Gigliotti, E. Boggio, N. Clemente, Y. Shivakumar, E. Toth, D. Sblattero, P. D'Amelio, G.C. Isaia, C. Dianzani, J. Yagi, J.M. Rojo, A. Chiocchetti, R. Boldorini, M. Bosetti, U. Dianzani, ICOS-Ligand Triggering Impairs Osteoclast Differentiation and Function In Vitro and In Vivo, J. Immunol. 197 (10) (2016) 3905-3916. DOI: 10.4049/jimmunol.1600424

[19] S. Acharya, S.K. Sahoo, PLGA nanoparticles containing various anticancer agents and tumour delivery by EPR effect, Adv. Drug Deliv. Rev. 63(3) (2011) 170-183.doi: 10.1016/j.addr.2010.10.008

[20] F. Trotta, M. Zanetti, R. Cavalli, Cyclodextrin-based nanosponges as drug carriers, Beilstein J. Org. Chem. 8 (2012) 2091-2099. DOI: 10.3762/bjoc.8.235.

[21] D. Ding, Q. Zhu, Recent advances of PLGA micro/nanoparticles for the delivery of biomacromolecular therapeutics, Mater. Sci. Eng. C. Mater. Biol. Appl. 92 (2018) 1041-1060. DOI: 10.1016/j.msec.2017.12.036.22.

[22] A. Jain, A. Jain, A. Gulbake, S. Shilpi, P. Hurkat, S.K. Jain, Peptide and protein delivery using new drug delivery systems, Crit. Rev. Ther. Drug Carrier Syst. 30 (4) (2013) 293-329.

[23] E. Boggio, C. Dianzani, C.L. Gigliotti, M.F. Soluri, N. Clemente, G. Cappellano, E. Toth, D. Raineri, B. Ferrara, C. Comi, U. Dianzani, A. Chiocchetti, Thrombin Cleavage of Osteopontin Modulates Its Activities in Human Cells In Vitro and Mouse Experimental Autoimmune Encephalomyelitis In Vivo, J. Immunol. Res. (2016) 2016:9345495. DOI: 10.1155/2016/9345495.

[24] X. Zhou, B. Liu, X. Yu, X. Zha, X. Zhang, X. Wang X, Y. Jin, Y. Wu, Y. Chen, Y. Shan, Y. Chen, J. Liu, W. Kong, J. Shen, Controlled release of PEI/DNA complexes from PLGA microspheres as a potent delivery system to enhance immune response to HIV vaccine DNA prime/MVA boost regime, Eur. J. Pharm. Biopharm. 68 (3) (2008) 589-595.

[25] K.L. DeCicco-Skinner, G.H. Henry, C. Cataisson, T. Tabib, J.C. Gwilliam, N.J. Watson, E.M. Bullwinkle, L. Falkenburg, R.C. O'Neill, A. Morin, J.S. Wiest JS, Endothelial cell tube formation assay for the in vitro study of angiogenesis, J. Vis. Exp. (91) (2014) e51312. DOI: 10.3791/51312.

[26] C.L. Gigliotti, R. Minelli, R. Cavalli, S. Occhipinti, G. Barrera, S. Pizzimenti, G. Cappellano, E. Boggio, L. Conti, R. Fantozzi, M. Giovarelli, F. Trotta, U. Dianzani, C. Dianzani, In Vitro and In Vivo Therapeutic Evaluation of Camptothecin-Encapsulated β-Cyclodextrin Nanosponges in Prostate Cancer, J. Biomed. Nanotechnol. 12 (1) (2016) 114-127.

[27] C. Passaro, F. Borriello, V. Vastolo, S. Di Somma, E. Scamardella, V. Gigantino, R. Franco, G. Marone, G. Portella, The oncolytic virus dl922-947 reduces IL-8/CXCL8 and MCP-1/CCL2 expression and impairs angiogenesis and macrophage infiltration inanaplastic thyroid carcinoma, Oncotarget 7 (2) (2016) 1500-1515. DOI:10.18632/oncotarget.6430.

[28] G. Cappellano, A.D. Woldetsadik, E. Orilieri, Y. Shivakumar, M. Rizzi, F. Carniato, C.L. Gigliotti, E. Boggio, N. Clemente, C. Comi, C. Dianzani, R. Boldorini, A. Chiocchetti, F. Renò, U. Dianzani, Subcutaneous inverse vaccination with PLGA particles loaded with a MOG peptide and IL-10 decreases

the severity of experimental autoimmune encephalomyelitis, Vaccine 32 (43) (2014) 5681-5689. DOI: 10.1016/j.vaccine.2014.08.016.

[29] J. Morimoto, S. Kon, Y. Matsui, T. Uede, Osteopontin; as a target molecule for the treatment of inflammatory diseases,Curr. Drug Targets 11 (4) (2010) 494-505.

[30] S. Swaminathan, R. Cavalli, F. Trotta, Cyclodextrin-based nanosponges: a versatile platform for cancer nanotherapeutics development. Wiley Interdiscip. Rev. Nanomed. Nanobiotechnol. 8 (4) (2016) 579-601. DOI: 10.1002/wnan.1384.

[31] F. Trotta, C. Dianzani, F. Caldera, B. Mognetti, R. Cavalli, The application of nanosponges to cancer drug delivery, Expert Opin. Drug Deliv, 11 (6) (2014) 931-941. DOI: 10.1517/17425247.2014.911729.

[32] M. Daga, C. Ullio, M. Argenziano, C. Dianzani, R. Cavalli, F. Trotta, C. Ferretti, G.P. Zara, C.L. Gigliotti, E.S. Ciamporcero, P. Pettazzoni, D. Corti, S. Pizzimenti, G. Barrera, GSH-targeted nanosponges increase doxorubicin-induced toxicity "in vitro" and "in vivo" in cancer cells with high antioxidant defenses, Free Radic. Biol. Med. 97 (2016) 24-37. DOI: 10.1016/j.freeradbiomed.

[33] M. Argenziano, C. Lombardi, B. Ferrara, F. Trotta, F. Caldera, M. Blangetti, H. Koltai, Y. Kapulnik, R. Yarden, C.L. Gigliotti, U. Dianzani, C. Dianzani, C. Prandi, R. Cavalli, Glutathione/pH-responsive nanosponges enhance strigolactone delivery to prostate cancer cells, Oncotarget 9 (88) (2018) 35813-35829. DOI: 10.18632/oncotarget.26287.

[34] F. Caldera, M. Argenziano, F. Trotta, C. Dianzani, C.L. Gigliotti, M. Tannous, L. Pastero, D. Aquilano, T. Nishimoto, T. Higashiyama, R. Cavalli, Cyclic nigerosyl-1,6-nigerose-based nanosponges: An innovative pH and time-controlled nanocarrier for improving cancer treatment, Carbohydr. Polym. 194 (2018) 111-121. DOI: 10.1016/j.carbpol.2018.04.027.

[35] C.L. Gigliotti, B. Ferrara, S. Occhipinti, E. Boggio, G. Barrera, S. Pizzimenti, M. Giovarelli, R. Fantozzi, A. Chiocchetti, M. Argenziano, N. Clemente, F. Trotta, C. Marchiò, L. Annaratone, R. Boldorini, U. Dianzani, R. Cavalli, C. Dianzani, Enhanced cytotoxic effect of camptothecin nanosponges

in anaplastic thyroid cancer cells in vitro and in vivo on orthotopic xenograft tumors, Drug Deliv. (1) (2017) 670-680. doi: 10.1080/10717544.2017.1303856.

[36] N. Clemente, M. Argenziano, C.L. Gigliotti, B. Ferrara, E. Boggio, A. Chiocchetti, F. Caldera, F. Trotta, E. Benetti, L. Annaratone, S. Ribero, S. Pizzimenti, G. Barrera, U. Dianzani, R. Cavalli, C. Dianzani, Paclitaxel-Loaded Nanosponges Inhibit Growth and Angiogenesis in Melanoma Cell Models, Front Pharmacol. (2019) 10:776. doi: 10.3389/fphar.2019.00776.

[37] R. Cavalli, F. Trotta, W. Tumiatti, L. Serpe, G.P. Zara, 5-Fluorouracil loaded β-cyclodextrin nanosponges: in vitro characterization and cytotoxicity, In: Proceedings XIII International Cyclodextrin Symposium, Turin, Italy, 14–17 May, 2006: 207.

[38] S.S. Darandale, P.R. Vavia, Cyclodextrin-based nanosponges of curcumin: formulation and physicochemical characterization, Journal of Inclusion Phenomena and Macrocyclic Chemistry April (2013) (75) 315–322.

[39] K.A. Ansari, P.R. Vavia, F. Trotta, R. Cavalli, Cyclodextrin-based nanosponges for delivery of resveratrol: in vitro characterisation, stability, cytotoxicity and permeation study, AAPS PharmSciTech. (2011) (1) 279-86. doi:10.1208/s12249-011-9584-3.

[40] F. Dilnawaz, S.K. Sahoo. Research paper: enhanced accumulation of curcumin and temozolomide loaded magnetic nanoparticles executes profound cytotoxic effect in glioblastoma spheroid model. Eur J Pharm Biopharm 2013, 85:452–462.

[41] Dora CP, Trotta F, Kushwah V, Devasari N, Singh C, Suresh S, Jain S. Potential of erlotinib cyclodextrin nanosponge complex to enhance solubility, dissolution rate, in vitro cytotoxicity and oral bioavailability. Carbohydr Polym. 2016 Feb 10;137:339-349. doi: 10.1016/j.carbpol.2015.10.080. Epub 2015 Oct 28.

[42] Shende P, Kulkarni YA, Gaud RS, Deshmukh K, Cavalli R, Trotta F, Caldera F. Acute and repeated dose toxicity studies of different β-cyclodextrin-based nanosponge formulations. J Pharm Sci. 2015 May;104(5):1856-63. doi: 10.1002/jps.24416. Epub 2015 Mar 9.

[43] Rawal S, Patel MM. Threatening cancer with nanoparticle aided combination oncotherapy. J Control Release. 2019 May 10;301:76-109. doi: 10.1016/j.jconrel.2019.03.015. Epub 2019 Mar 16.

[44] Song, W., Musetti, S. N., & Huang, L. (2017). Nanomaterials for cancer immunotherapy. Biomaterials, 148, 16-30.

[45] Joshi S, Durden DL. Combinatorial Approach to Improve Cancer Immunotherapy: Rational Drug Design Strategy to Simultaneously Hit Multiple Targets to Kill Tumor Cells and to Activate the Immune System. J Oncol. 2019 Feb 3;2019:5245034. doi: 10.1155/2019/5245034. eCollection 2019.

[46] Peres C, Matos AI, Conniot J, Sainz V, Zupančič E, Silva JM, Graça L, Sá Gaspar R, Préat V, Florindo HF. Poly(lactic acid)-based particulate systems are promising tools for immune modulation. Acta Biomater. 2017 Jan 15;48:41-57. doi: 10.1016/j.actbio.2016.11.012. Epub 2016 Nov 4.

[47] Varypataki EM, Silva AL, Barnier-Quer C, Collin N, Ossendorp F, Jiskoot W. Synthetic long peptide-based vaccine formulations for induction of cell mediated immunity: A comparative study of cationic liposomes and PLGA nanoparticles. J Control Release. 2016 Mar 28;226:98-106. doi: 10.1016/j.jconrel.2016.02.018. Epub 2016 Feb 11.

[48] Sau S, Alsaab, HO, Bhise K, Alzhrani R, Nabil G, Iyer AK. Multifunctional nanoparticles for cancer immunotherapy: A groundbreaking approach for reprogramming malfunctioned tumor environment. J Control Rel. 2018; 274, 24-34.

[49] Conniot J, Scomparin A, Peres C, Yeini E, Pozzi S, Matos AI, Kleiner R, Moura LIF, Zupančič E, Viana AS, Doron H, Gois PMP, Erez N, Jung S, Satchi-Fainaro R, Florindo HF. Immunization with mannosylated nanovaccines and inhibition of the immune-suppressing microenvironment sensitizes

melanoma to immune checkpoint modulators. Nat Nanotechnol. 2019 Aug 5. doi: 10.1038/s41565-019-0512-0.

[50] Danhier F, Ansorena E, Silva JM, Coco R, Le Breton A, Préat V. PLGA-based nanoparticles: an overview of biomedical applications. J Control Release. 2012 Jul 20;161(2):505-22. doi: 10.1016/j.jconrel.2012.01.043. Epub 2012 Feb 4.

[51] Rezvantalab S, Drude NI, Moraveji MK, Güvener N, Koons EK, Shi Y, Lammers T, Kiessling F. PLGA-Based Nanoparticles in Cancer Treatment. Front Pharmacol. 2018 Nov 2;9:1260. doi: 10.3389/fphar.2018.01260. eCollection 2018.

[52] I. Papa, D. Saliba, M. Ponzoni, S. Bustamante, P.F. Canete, P. Gonzalez-Figueroa, H.A. McNamara, S. Valvo, M. Grimbaldeston, R.A. Sweet, H. Vohra, I.A. Cockburn, M. Meyer-Hermann, M.L. Dustin, C. Doglioni, C.G. Vinuesa, T(FH)-derived dopamine accelerates productive synapses in germinal centres, Nature 547 (7663) (2017) 318-323. DOI: 10.1038/nature23013.

[53] H. Wiendl, M. Mitsdoerffer, D. Schneider, A. Melms, H. Lochmuller, R. Hohlfeld, M. Weller, Muscle fibres and cultured muscle cells express the B7.1/2-related inducible co-stimulatory molecule, ICOSL: implications for the pathogenesis of inflammatory myopathies, Brain 126 (Pt 5) (2003) 1026-1035.

[54] L. Mo, Q. Chen, X. Zhang, X. Shi, L. Wei, D. Zheng, H. Li, J. Gao, J. Li, Z. Hu, Depletion of regulatory T cells by anti-ICOS antibody enhances anti-tumor immunity of tumor cell vaccine in prostate cancer, Vaccine 35 (43) (2017) 5932-5938. DOI: 10.1016/j.vaccine.2017.08.093.

[55] K.S. Le, M.L. Thibult, S.Just-Landi, S. Pastor, F. Gondois-Rey, S. Granjeaud, F. Broussais, R. Bouabdallah, R.Colisson, C.Caux, C. Ménétrier-Caux, D. Leroux, L. Xerri, D. Olive, Follicular B Lymphomas Generate Regulatory T Cells via the ICOS/ICOSL Pathway and Are Susceptible to Treatment by Anti-ICOS/ICOSL Therapy, Cancer Res. 76 (16) (2016)4648-4660. DOI: 10.1158/0008-5472.CAN-15-0589.

[56] F. Amatore, L. Gorvel, D. Olive, Inducible Co-Stimulator (ICOS) as a potential therapeutic target for anti-cancer therapy, Expert Opin. Ther. Targets 22 (4) (2018) 343-351. DOI: 10.1080/14728222.2018.1444753.

[57] O. Marinelli, M. Nabissi, M.B. Morelli, L. Torquati, C. Amantini, G. Santoni, ICOS-L as a Potential Therapeutic Target for Cancer Immunotherapy, Curr. Protein Pept. Sci. 19 (11) (2018) 1107-1113. DOI: 10.2174/1389203719666180608093913.

[58] Xu J, Ren X, Guo T, Sun X, Chen X, Patterson LH, Li H, Zhang J. NLG919/cyclodextrin complexation and anti-cancer therapeutic benefit as a potential immunotherapy in combination with paclitaxel. Eur J Pharm Sci. 2019 Oct 1;138:105034. doi: 10.1016/j.ejps.2019.105034. Epub 2019 Aug 2.

[59] Park J, Wrzesinski SH, Stern E, Look M, Criscione J, Ragheb R, Jay SM, Demento SL, Agawu A, Licona Limon P, Ferrandino AF, Gonzalez D, Habermann A, Flavell RA, Fahmy TM. Combination delivery of TGF-β inhibitor and IL-2 by nanoscale liposomal polymeric gels enhances tumour immunotherapy. Nat Mater. 2012 Oct;11(10):895-905. doi: 10.1038/nmat3355. Epub 2012 Jul 15.

Figure captions

Fig. 1. Characterization of CDNS formulations. (a) CDNS size distribution was determined using NanoSight Nanoparticle Tracking Analysis (NTA). (b) Field-emission scanning electron microscopy (FESEM) image of ICOS-Fc loaded CDNS (scale bar 500 nm). (c) *In vitro* release kinetics of ICOS-Fc from ICOS-Fc loaded CDNS upon incubation at 37°C, evaluated by BCA assay. (d) *In vitro* evaluation of ICOS-Fc stability over time upon storing at 4°C, evaluated by BCA assay (n=3). (e) Effect of free ICOS-Fc (ICOS-Fc), empty CDNS (CDNS), and CDNS loaded with ICOS-Fc on viability of B16-F10 cells evaluated after a 72 hr incubation with 2 and 5 μg/ml of ICOS-Fc (either free or loaded in CDNS); the empty CDNS samples contained CDNS amounts comparable to those present in the corresponding CDNS/ICOS-Fc doses (n=5); $^{**}P<0.01$ *vs* free ICOS-Fc and empty CDNS.

Fig. 2. Effect of different formulations of ICOS-Fc on the growth of B16-F10 tumors in C57BL6/J wild-type mice. C57BL6/J wild-type mice with palpable subcutaneous B16-F10 tumors were treated every 4 days with saline (CTR, black diamonds), CDNS alone (black squares), ICOS-Fc (black circles) or CDNS loaded with ICOS-Fc (black triangles). Tumor volume (cm^3) was evaluated every four days after the first treatment (T0, when the tumor was palpable). Each treatment involved 5 mice *per* experiment ($^{**}P\leq0.01$ *vs* control values).

Fig. 3. Effect of CDNS-ICOS-Fc on B16-F10 tumor growth on Treg markers *ex vivo* and angiogenesis *in vivo* (a) C57BL6/J wild-type mice with palpable subcutaneous B16-F10 tumors were treated and analyzed as described in the legend to fig. 2. Saline (CTR, black diamonds), CDNS alone (black squares), and CDNS loaded with ICOS-Fc (black triangles). Each treatment involved 5 mice/experiment. (b) Expression levels of IL-10 and FoxP3, were evaluated by RT-PCR in lysates from

tumor masses. The data are normalized for the expression of each gene in control mice (set at 100%); (n=5). (c) Immunofluorescence staining for anti-CD31 of tumors tissue sections from mice treated with saline (CTR), CDNS alone or CDNS loaded with ICOS-Fc. The slides were stained with a rabbit α-mouse CD31 Ab plus a secondary α-rabbit antibody conjugated with Alexa Fluor® 488. Microphotographs of CD31 staining from a representative experiment (green; magnification 200x). Graph shows tumor microvessel density (TMD) determined as the percentage of CD31-positive area on the tumor sections. Three randomly selected areas from three tumors from each group were analyzed. (*P<0.05, **$P\leq$ 0.01 *vs* control values).

Fig. 4. Effect of ICOS-Fc on the growth of B16-F10 tumors in ICOS-deficient mice. Mice with palpable subcutaneous B16-F10 tumors were treated every 4 days with saline (CTR, black diamonds), CDNS alone (black squares) or CDNS loaded with ICOS-Fc (black triangles). (a) Tumor volumes (cm^3) were evaluated every four days after the first treatment performed at T0 (i.e. when the tumor was palpable); each group involved 8 mice. (b) Expression of IL-10 and FoxP3 mRNA levels in tumor lysates measured by RT-PCR; values are normalized for basal expression in the control group set at 100%. (c) Microphotographs of CD31 staining from a representative experiment (green, magnification 200x); the graph shows the TMD determined as the percentage of CD31-positive area calculated as described in the legend to Fig.3c. (*P<0.05, **$P\leq$0.01 *vs* control values).

Fig. 5. Characterization of PLGA NP formulations. (a) Field-emission scanning electron microscopy (FESEM) image of ICOS-Fc loaded PLGA NPs (scale bar 500 nm). (b) PLGA NP size distribution determined using NanoSight Nanoparticle Tracking Analysis (NTA). (c) *In vitro* release kinetics of ICOS-Fc from ICOS-Fc loaded PLGA NPs upon incubation at 37°C, evaluated by BCA assay. (d) *In vitro* evaluation of ICOS-Fc stability over time upon storing at 4°C, evaluated by BCA assay (n=3).

Fig. 6. Effect of ICOS-Fc encapsulated on PLGA on the growth of B16-F10 tumors in C57BL6/J wild-type mice. (a-c) Mice with palpable subcutaneous B16-F10 tumors were treated every 4 days with saline (CTR, black diamonds), PLGA alone (black squares) or PLGA loaded with ICOS-Fc (black triangles). (a) Graph shows the tumor volume curves (cm^3); tumors were evaluated every four days after the first treatment performed at T0 (i.e. when the tumor was palpable); each treatment involved 8 mice. (b) Microphotographs of CD31 staining from a representative experiment (green; magnification 200x); the graph shows TMD determined as the percentage of CD31-positive area calculated as described in the legend to Fig. 3c. (c) Expression of IL-10 and FoxP3 in tumor lysates analyzed by RT-PCR; values are normalized for the expression in the control group set at 100%. (d) Mice with palpable subcutaneous B16-F10 tumors were treated with a single dose of each treatment at T0; graph shows the tumor volume curves (cm^3) evaluated as in (a); each treatment involved 8 mice; photographs show representative tumors. (*$P<0.05$, **$P\leq0.01$, from the respective control values).

Fig. 7. Effect of ICOS-Fc on HUVEC tubulogenesis *in vitro*. For tube formation assay, HUVECs were treated, maintained, and cultured in the presence or absence of OPN (25 μg/ml) or VEGF-α (10 ng/ml) with or without ICOS-Fc (25 μg/ml), as indicated. The morphology of capillary-like structures formed by HUVECs was analyzed 6 h after culturing using an inverted microscope. (a) Panels show a representative tubulogenesis experiment photographed with a digital camera (magnification 10x). (b) The results are expressed as number of tubes *per* three wells cultured in each condition (n=3) (**$P\leq0.01$ *vs* control values). The horizontal line (NT) shows tube formation of HUVEC in the absence of the angiogenic stimuli.